Separation Science and Technology
Publication details, including instructions for authors and subscription information:
http://www.informaworld.com/smpp/title~content=t713708471

Selective Cu^2 and Pb^2 Exchange with Highly Charged Cation Exchanger of Na-4-Mica

Tatsuya Kodama[a]; Sridhar Komarneni[b]
[a] Department of Chemistry & Chemical Engineering, Faculty of Engineering, Niigata University, Niigata, Japan [b] MATERIALS RESEARCH LABORATORY AND DEPARTMENT OF AGRONOMY, THE PENNSYLVANIA STATE UNIVERSITY, UNIVERSITY PARK, PENNSYLVANIA, USA

Online publication date: 16 August 1999

To cite this Article Kodama, Tatsuya and Komarneni, Sridhar(1999) 'Selective Cu^2 and Pb^2 Exchange with Highly Charged Cation Exchanger of Na-4-Mica', Separation Science and Technology, 34: 12, 2275 — 2292
To link to this Article: DOI: 10.1081/SS-100100772
URL: http://dx.doi.org/10.1081/SS-100100772

SEPARATION SCIENCE AND TECHNOLOGY, **34**(12), pp. 2275–2292, 1999

Selective Cu^{2+} and Pb^{2+} Exchange with Highly Charged Cation Exchanger of Na-4-Mica

TATSUYA KODAMA* and SRIDHAR KOMARNENI†
MATERIALS RESEARCH LABORATORY AND DEPARTMENT OF AGRONOMY
THE PENNSYLVANIA STATE UNIVERSITY
UNIVERSITY PARK, PENNSYLVANIA 16802, USA

ABSTRACT

Selective cation exchange for Cu and Pb has been demonstrated with the high-charge-density sodium fluorophlogopite mica, Na-4-mica. The $2Na^+ \rightarrow M^{2+}$ exchange reaction (M = Cu or Pb) was investigated with Na-4-micas prepared by two different synthetic processes. One was easily and economically prepared by crystallization from a mixture of NaF, MgO, and metakaolin, the latter serves as an inexpensive aluminosilicate source. Another was prepared by solution–sol–gel processing. Ion-exchange isotherms for Cu^{2+} and Pb^{2+} were obtained at room temperature. The thermodynamic functions for the initial ion-exchange reactions were calculated because the isotherms were not completed. High selectivities for both copper and lead exchange were found on the highly crystallized Na-4-mica prepared from metakaolin. Their ion-exchange capacities were 225 and 257 milliequivalents per 100 g of dry clay for Cu^{2+} and Pb^{2+}, respectively. This high level decontamination of copper and lead with the highly crystallized Na-4-mica from metakaolin will be a very important separation required for purification of drinking water as well as for wastewater treatment and disposal.

INTRODUCTION

Synthetic and naturally occurring clays form a large family of inorganic ion exchangers which have numerous applications including their extensive use in recovery of metals from waste solution and wastewater treatment and disposal (1). Mica is one of the most representative of 2:1 phyllosilicates, i.e., each layer

* Permanent address: Department of Chemistry & Chemical Engineering, Faculty of Engineering, Niigata University, 8050 Ikarashi 2-nocho, Niigata 950-21, Japan.
† To whom correspondence should be addressed.

consisting of an octahedral sheet sandwiched between two tetrahedral sheets. The considerable differences in properties of phyllosilicates can be related to the chemical composition of the 2:1 layer, which determines such important parameters as the layer charge and its distribution, as well as the dimensions and the geometrical details for the different parts of the layer. Substitution of Al^{3+} for Si^{4+} in the tetrahedral sheets of micas is the main mechanism which generates a negative layer charge, and this is balanced by cations in the interlayers. Micas have the largest layer charge density among the 2:1 phyllosilicate clay minerals (2). The two main categories of micas based on layer charge density are 1) true micas with 1 negative charge per formula unit and 2) brittle micas with 2 negative charges per formula unit.

A highly charged sodium fluorophlogopite mica, $Na_4Mg_6Al_4Si_4O_{20}F_4 \cdot xH_2O$, analogous to brittle micas, was first prepared by Gregorkiewitz et al. in 1974; it was informally named Na-4-mica (3). The ion-exchange capacities of clay minerals, such as the smectite and kaolinite types, are frequently less than 100 milliequivalents (mequiv) per 100 g of dry clay (2). However, the Na-4-mica has a theoretical ion-exchange capacity of 468 mequiv $(100\ g)^{-1}$ on an anhydrous basis. Thus this phase extends the range of interesting clay minerals as an inorganic cation exchanger (3–7). The preliminary characterization of Na-4-mica leads to the postulation of a trioctahedral 2:1 layer, similar to those in fluorphlogopite, but with an unusually high Al-Si substitution in the tetrahedral sheet. For the compensation of the high layer charge, this mica contains an unusually large number of 4 interlayer monovalent ions of sodium per unit cell. No mica with more than 2 interlayer cations per unit cell had ever been observed before. The Na-4-mica is unique among micas because it becomes hydrated on contact with water or even in air at ambient conditions. The presence of an unusually large number of interlayer cations and a resulting offset layer stacking by $\frac{1}{3}b$ allows the structure to expand from a dehydrated 9.81 Å to a hydrated 12.18 Å *c*-axis spacing to achieve a more thermodynamically stable interlayer structure. Hydration of the interlayer space facilitates cation diffusion and exchange in the interlayers of this special swelling mica.

A very fine and pure phase of the Na-4-mica which is essential for practical applications was previously prepared by a solution–sol–gel processing using tetraethoxysilane, aluminum nitrate, and magnesium nitrate (4), and was shown to have high ion-exchange selectivities for many divalent transition-metal ions and for strontium and barium, but not for the alkali-metal ions, magnesium, and calcium (5). A simplified procedure was later developed for the synthesis of this mica using fumed silica as the silica source (6). For waste disposal or metals recovery applications, it is necessary to develop an even more cost-effective synthetic process for Na-4-mica.

We have recently reported the synthesis of Na-4-mica using calcined kaolinite (metakaolin) as an economical aluminosilicate source (7). Highly crys-

MARCEL DEKKER, INC.
270 Madison Avenue, New York, New York 10016

talline Na-4-mica was obtained easily and economically from a mixture of NaF, MgO, and metakaolin at 850–890°C. The present work describes the selective cation exchange of copper and lead in two Na-4-micas, one synthesized using metakaolin and another using aluminosilicate gel. These basic studies are of relevance in the decontamination of copper and lead from drinking as well as wastewater.

EXPERIMENTAL

Preparation of Na-4-micas

Na-4-mica samples were prepared by two different methods: one was the solution–sol–gel processing previously reported (4). The procedure is briefly outlined as follows. A monophasic gel powder was prepared by separately dissolving $Al(NO_3)_3 \cdot 9H_2O$ and $Mg(NO_3)_2 \cdot 6H_2O$ in absolute ethanol and then combining and mixing the two solutions for an hour with stirring. A known quantity of tetraethylorthosilicate, $Si(OC_2H_5)_4$, was added to obtain a stoichiometric composition of the mixture, which when reduced to pure oxides was $3MgO\text{-}Al_2O_3\text{-}2SiO_2$. The resulting sol was stirred for 3 hours to ensure homogeneity, then tightly covered and placed in a 60°C oven to promote hydrolysis, condensation, and polymerization reactions for 3 days. The water of hydration of Al and Mg nitrates is sufficient for hydrolysis and therefore no water was added. This resulted in a single-phase gel which was then dried at 100°C in an oven, calcined at 475°C for 12 hours, ground to pass through a −325 mesh screen, and intimately mixed with an equal mass of −325 mesh crystalline NaF. The mixture was heated for 18 hours at 890°C in a platinum vessel in air using a programmed furnace.

Another Na-4-mica sample was prepared from a mixture of MgO, NaF, and calcined kaolinite (metakaolin). Naturally occurring kaolinite has the desired 1:1 Si to Al molar ratio in its theoretical chemical composition $Al_2Si_2O_5(OH)_4 \cdot nH_2O$, and serves as a good aluminosilicate source for the synthesis of Na-4-mica. A poorly crystallized kaolinite of composition 47.9% SiO_2, 38.3% Al_2O_3, 2.08% TiO_2, 0.98% Fe_2O_3, 0.15% FeO, and 0.03% MgO (supplied by Georgia Kaolin Company through W. D. Johns, Department of Geology, University of Missouri, Columbia, MO 65201, USA), ultrafine MgO (supplied by Ube Industries, Ube, Japan), and NaF were the starting materials for the synthesis of the Na-4-mica. The poorly crystallized kaolinite was first calcined at 700°C for 18 hours to transform it to an amorphous product, metakaolin ($Al_2Si_2O_7$), by dehydration and dehydroxylation. The metakaolin was cooled and stored in a desiccator over silica gel at room temperature. The water contents of metakaolin and ultrafine MgO were determined by thermal analysis using TG DTA 2010, Mac Science. Appropriate proportions of the ultrafine MgO and the metakaolin were mixed to obtain a

stoichiometric composition. Then it was mixed with an equal mass of NaF and transferred to a platinum vessel. The mixture was heated for 6 hours at 890°C in air using a programmed furnace.

The resulting solids prepared by the above two different methods were ground up and washed in deionized water several times to remove excess NaF. Any remaining impurity phases, such as insoluble fluoride salts, were then removed with repeated washings using saturated boric acid solution. The products were again washed with deionized water and dried at 60°C in an oven for 2–3 days. The Na-4-micas thus prepared were finally stored in a desiccator over silica gel at room temperature. Although assynthesized Na-4-mica was anhydrous, the washed sample hydrated readily. Hereafter the Na-4-mica prepared from metakaolin is referred as metakao-Na-4-mica and the solution–sol–gel processed Na-4-mica as solgel-Na-4-mica.

Powder x-ray diffraction (XRD) was carried out to check for phase purity, to determine the basal spacings of the Na-4-mica, and to monitor crystallinity using a Rigaku RAD-rA diffractometer with CuKα radiation. Scanning electron microscopy (SEM) was used to determine particle size and shape. An ISI-DS 130 instrument was used for SEM. Water contents of the hydrated Na-4-micas were determined by thermal analysis to be $Na_4Mg_6Al_4Si_4O_{20}F_4 \cdot 2.8H_2O$ and $Na_4Mg_6Al_4Si_4O_{20}F_4 \cdot 2.6H_2O$ for solgel-Na-4-mica and metakao-Na-4-mica, respectively.

Cation-Exchange Isotherm Determination

The $2Na^+ \rightarrow M^{2+}$ (M = Cu and Pb) exchange reaction was performed with the two different ion-exchanger samples of solgel-Na-4-mica and metakao-Na-4-mica. A 25-mg portion of the Na-4-mica (anhydrous basis) was equilibrated with 25 cm^3 of the mixed solution having different mole ratios of Na^+/M^{2+} with shaking at 25°C for 4 weeks. The total normality of the solutions was kept constant at 0.00468 N (Na^+/M^{2+} = 0.0–0.9). The total normalities of 0.00585 and 0.00702 N were additionally used for $2Na^+ \rightarrow Cu^{2+}$ exchange with the metakao-Na-4-mica. To avoid the hydrolysis of cations in the solution and the precipitation of metal hydroxides and oxides, the pH of the solutions was set to 3.0 by adding HCl solution prior to the ion-exchange reaction. The pH of the solution increased in a few minutes to about 4 upon equilibration with mica. After equilibration, the supernatant solution was analyzed for the divalent metal ions by atomic emission spectroscopy (SpectraSpan III instrument). The amounts of metal ions exchanged or released by Na-4-mica were determined from the difference in the concentration between the sample solution and the reference. The theoretical cation-exchange capacity [468 mequiv $(100\ g)^{-1}$ of anhydrous form] was used for representing the ion-exchange isotherm.

MARCEL DEKKER, INC.
270 Madison Avenue, New York, New York 10016

THEORETICAL

The mono-divalent ion exchange process in the Na-4-mica is represented by

$$2\overline{Na}^{+} + M^{2+} \leftrightharpoons 2Na^{+} + \overline{M}^{2+} \tag{1}$$

where the bar above the symbols represents the ion-exchanger phase. The thermodynamic equilibrium constant, **K,** of the reversible ion-exchange reaction is defined by

$$\mathbf{K} = \frac{[Na^{+}]^2 \overline{X}_M \gamma_{Na}^2 f_M}{[M^{2+}]\overline{X}_{Na}^2 \gamma_M f_{Na}^2} \tag{2}$$

where $[Na^{+}]$ and $[M^{2+}]$ are molalities or molarities of the ions in solution, and γ_i and f_i are activity coefficients in the solution phase and in the ion-exchanger phase, respectively. The standard states are taken for the ion-exchanger phase as the exchanger is in its pure Na^{+} form and pure M^{2+} form, and the activity coefficients, f_{Na} and f_M, are chosen as unity when the exchanger is at the standard state of the Na^{+} form and the M^{2+} form, respectively. γ_{Na} and γ_M are unity when $[Na^{+}]$ and $[M^{2+}]$ approach zero. $\overline{X}_i$ is an equivalent fraction of ion i in the ion-exchanger phase, defined by

$$\overline{X}_{Na} = \frac{[\overline{Na}^{+}]}{2[\overline{M}^{2+}] + [\overline{Na}^{+}]}, \qquad \overline{X}_M = \frac{2[\overline{M}^{2+}]}{2[\overline{M}^{2+}] + [\overline{Na}^{+}]} \tag{3}$$

The molarities $[Na^{+}]$ and $[M^{2+}]$ can be replaced by the equivalent fractions of the ions in the solution (X_i):

$$X_{Na} = \frac{[Na^{+}]}{2[M^{2+}] + [Na^{+}]}, \qquad X_M = \frac{2[M^{2+}]}{2[M^{2+}] + [Na^{+}]} \tag{4}$$

$$[Na^{+}] + 2[M^{2+}] = TN \tag{5}$$

where TN represents the total normality of the solution. Using a corrected selectivity coefficient, $\mathbf{K}_{Na}^{M}$, the thermodynamic equilibrium constant is rewritten as (8)

$$\mathbf{K} = \mathbf{K}_{Na}^{M} \frac{f_M}{f_{Na}^2} \tag{6}$$

where

$$\mathbf{K}_{Na}^{M} = \frac{X_{Na}^2 \overline{X}_M \gamma_{Na}^2}{X_M \overline{X}_{Na}^2 \gamma_M} [2(TN)] \tag{7}$$

When the total normality, $TN = [Na^+] + 2[M^{2+}]$, is lower than 0.01 N, γ^2_{Na}/γ_M will be close to unity. As shown by Eq. (7), the corrected selectivity coefficient is dependent on the total normality.

A corrected selectivity coefficient larger than unity ($\ln \mathbf{K}^M_{Na} > 0$) indicates selectivity for the ion M^{2+} (9). Na^+ ions are more preferred if $\mathbf{K}^M_{Na}$ is smaller than unity ($\ln \mathbf{K}^M_{Na} < 0$). When $\mathbf{K}^M_{Na}$ is equal to unity ($\ln \mathbf{K}^M_{Na} = 0$), no preference between these ions is indicated.

The corrected selectivity coefficient, $\mathbf{K}^M_{Na}$, is related to the Kielland coefficient as given below. Kielland plots show the details of the ion-exchange selectivity as a function of the equivalent fraction, $\overline{X}_M$ (10).

$$\log \mathbf{K}^M_{Na} = \sum_{m=1} (m+1) C_m \overline{X}^m_M + \log(\mathbf{K}^M_{Na})_{\overline{X}_M \to 0} \tag{8}$$

where the coefficient, C_m, is called generalized Kielland coefficient. These plots often give linear relationships with a slope $2C_1$, in which case Eq. (8) can become

$$\log \mathbf{K}^M_{Na} = 2\mathbf{C}_1 \overline{X}_M + \log(\mathbf{K}^M_{Na})_{\overline{X}_M \to 0} \tag{9}$$

If the Gibbs–Duhem equation is applied to the ion-exchange reaction, the thermodynamic equilibrium constant, K, is given by the integration of the Kielland plot from $\overline{X}_M = 0$ to $\overline{X}_M = 1$ (11, 12).

$$\ln \mathbf{K} = (Z_{Na} - Z_M) + \int_0^1 \ln \mathbf{K}^M_{Na} d\overline{X}_M + \Delta \tag{10}$$

Here, Z_{Na} and Z_M are the number of charges on the Na^+ and M^{2+}. The third term on the right, Δ, is negligible when compared with experimental accuracy in measuring the equilibrium (8). Equations (9) and (10) are combined to give the thermodynamic constant K:

$$\ln \mathbf{K} = (Z_{Na} - Z_M) + 2.303 C_1 + \ln(\mathbf{K}^M_{Na})_{\overline{X}_M \to 0} \tag{11}$$

Thus, the thermodynamic equilibrium constant is determined by the valences of the exchanging cations, the generalized Kielland coefficient C_1, and the intercept of the Kielland plot, $(\mathbf{K}^M_{Na})_{\overline{X}_M \to 0}$. The Gibbs standard free energy change, $\Delta G°$, can be calculated by,

$$\Delta G° = -RT \ln K \tag{12}$$

The generalized Kielland coefficient, C_1, is related to the energy term for the steric limitation or jumping barrier for exchanging ions in the interlayer (13, 14). Generally, the C_1 value is negative, and the energy term for the steric limitation is larger as the $|C_1|$ value is larger. When the C_1 value is zero, the corrected selectivity coefficient can be used as an index of the ion-exchange selectivity for "ideal" exchange with no steric hindrance (15, 16).

$$\ln \mathbf{K}_{\text{ideal}} = (Z_{\text{Na}} - Z_{\text{M}}) + \ln(\mathbf{K}^{\text{M}}_{\text{Na}})_{\overline{X}_{\text{M}} \to 0} \quad (13)$$

The Gibbs standard free energy change for "ideal exchange" is given by

$$\Delta G^{\circ}_{\text{ideal}} = -RT \ln K_{\text{ideal}} \quad (14)$$

RESULTS AND DISCUSSION

Materials

Figure 1 shows XRD patterns of the resultant Na-4-micas prepared by solution–sol–gel processing (solgel-Na-4-mica) and by calcination of the mixture of metakaolin, MgO, and NaF (metakao-Na-4-mica). That a Na-4-mica was synthesized was evident from the presence of the first-order (001) reflection in the XRD pattern. In the XRD pattern of the solgel-Na-4-mica, a strong but broadened peak was observed around $d = 12.2$ Å, which corresponds to a

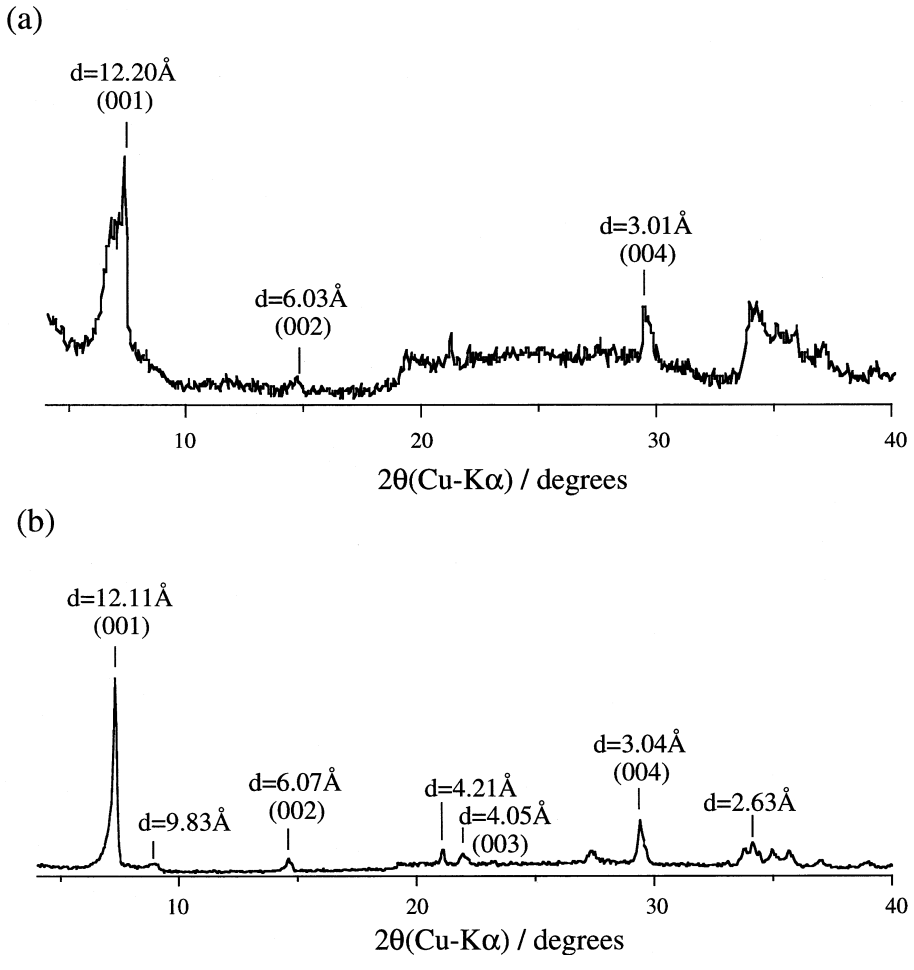

FIG. 1 XRD patterns of the Na–4–micas prepared (a) by solution–sol–gel processing and (b) by crystallization from the mixture of NaF, MgO, and metakaolin precursors.

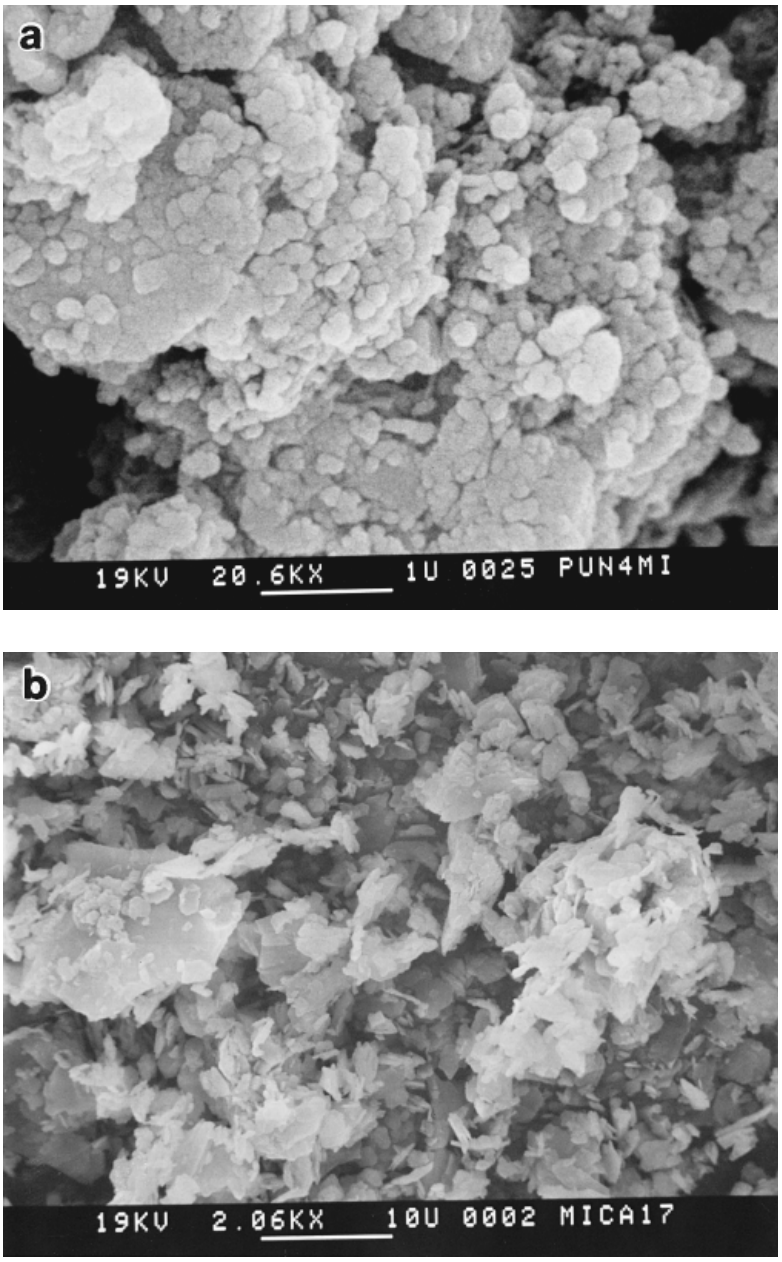

FIG. 2 SEM micrographs of the Na–4–micas prepared (a) by solution–sol–gel processing and (b) by crystallization from the mixture of NaF, MgO, and metakaolin precursors.

basal spacing of the hydrated form of Na-4-mica with a structure of a single sheet of interlayer water (3–7). For the metakao-Na-4-mica, a very strong and sharp peak was observed at $d = 12.1$ Å, suggesting the higher crystallinity of the metakao-Na-4-mica in comparison with that of the solgel-Na-4-mica. In the metakao-Na-4-mica, the small peak observed at $d = 9.8$ Å is due to a basal spacing of the anhydrous form. Small peaks observed at $d = 6.06$, 4.05, and

3.03 Å are assigned to (002), (003), and (004) reflections of *c*-axis spacing of the hydrated form with a single interlayer water sheet, which were more definitely observed for the metakao-Na-4-mica. Specific characteristic peaks observed at $d = 4.21$ and 2.63 Å are almost consistent with the limited powder XRD data previously reported by Franklin et al. (6). An almost pure phase of Na-4-mica was synthesized both by solution–sol–gel processing and by calcination of the mixture of metakaolin, MgO, and NaF. A very highly crystallized Na-4-mica could be especially prepared by the latter method. Kaolinite is a 1:1 phyllosilicate, belonging to the dioctahedral subgroup. The high crystallinity of metakao-Na-4-mica may be because Na-4-mica is favorably crystallized in the matrix of a skeleton structure of metakaolin as a precursor of Al and Si mixed at the atomic level.

The crystal shapes and sizes of these Na-4-micas are clearly seen in Fig. 2. The SEM micrographs showed that the Na-4-micas have pseudohexagonal crystallites. The crystallite size of metakao-Na-4-mica ranges between 2 and 10 μm, with many crystallites around 3–4 μm in size. The solgel-Na-4-mica has a smaller crystallite size of around 0.2–0.4 μm.

$2Na^{+} \rightarrow Cu^{2+}$ Exchange with the Na-4-micas

The isotherms for $2Na^{+} \rightarrow Cu^{2+}$ exchange with the two different Na-4-micas are shown in Fig. 3 as the equivalent fraction of the divalent metal in the

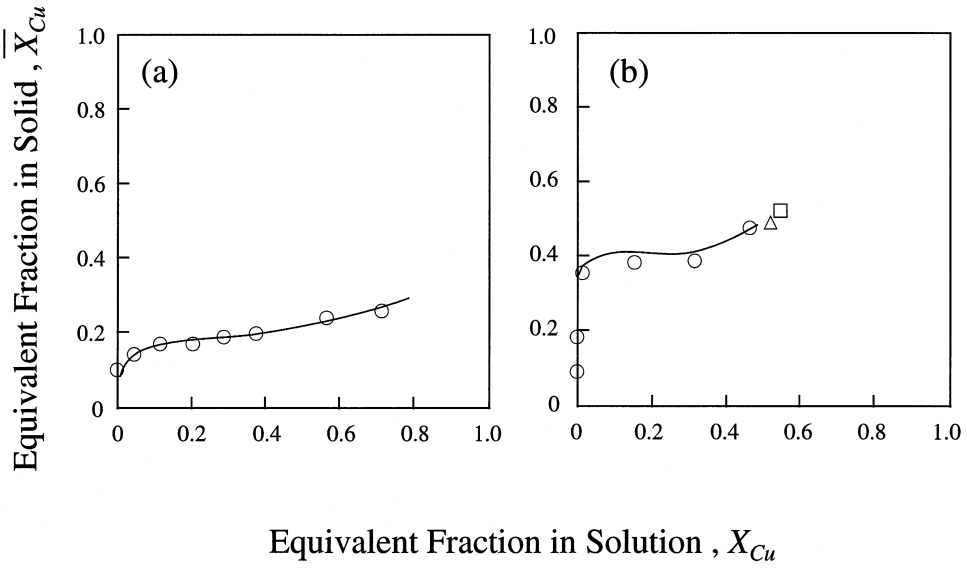

FIG. 3 Cation-exchange isotherms for $2Na^{+} \rightarrow Cu^{2+}$ exchange on the two different Na–4–micas prepared (a) by solution–sol–gel processing and (b) by crystallization from the mixture of NaF, MgO, and metakaolin precursors. Total normalities of 0.00468 N (circles), 0.00585 N (triangles), and 0.00702 N (squares) were used.

Na-4-mica phase against the equivalent cation fraction in the solution. For the solgel-Na-4-mica, the copper-exchange isotherm quickly flattens out when the equivalent fraction of Cu^{2+} in the mica reaches $\overline{X}_{Cu} = 0.17$. Its copper-exchange capacity at $TN = 0.00468$ N, 122 mequiv $(100\ g)^{-1}$, is only 26% of the theoretical exchange capacity of Na-4-mica. The copper-exchange isotherm with the metakao-Na-4-mica also quickly flattens out, but the equivalent fraction of Cu^{2+} in the mica quickly reaches $\overline{X}_{Cu} = 0.36$. Its copper-exchange capacity at $TN = 0.00468$ N was much improved to 225 mequiv $(100\ g)^{-1}$, which is 48% of the theoretical exchange capacity of Na-4-mica. The selectivity for Cu^{2+} of the Na-4-mica was much improved with the highly crystallized metakao-Na-4-mica. Figure 4 shows the Kielland plots for the $2Na^{+} \rightarrow Cu^{2+}$ exchange with the two different Na-4-micas. The Kielland plots both gave a linear relation, indicating that the copper-exchange reaction proceeds on one kind of exchangeable site of Na-4-mica, which is the interlayer Na^{+} site. The dotted lines in Fig. 4 indicate that the corrected selectivity coefficient is equal to unity. For the metakao-Na-4-mica, the Kielland plots fall above the dotted line at $\overline{X}_{Cu} < 0.3$, indicating selectivity for Cu^{2+}. At $\overline{X}_{Cu} > 0.3$, however, Na^{+} ions are more preferred than Cu^{2+}. For the solgel-Na-4-mica, all the

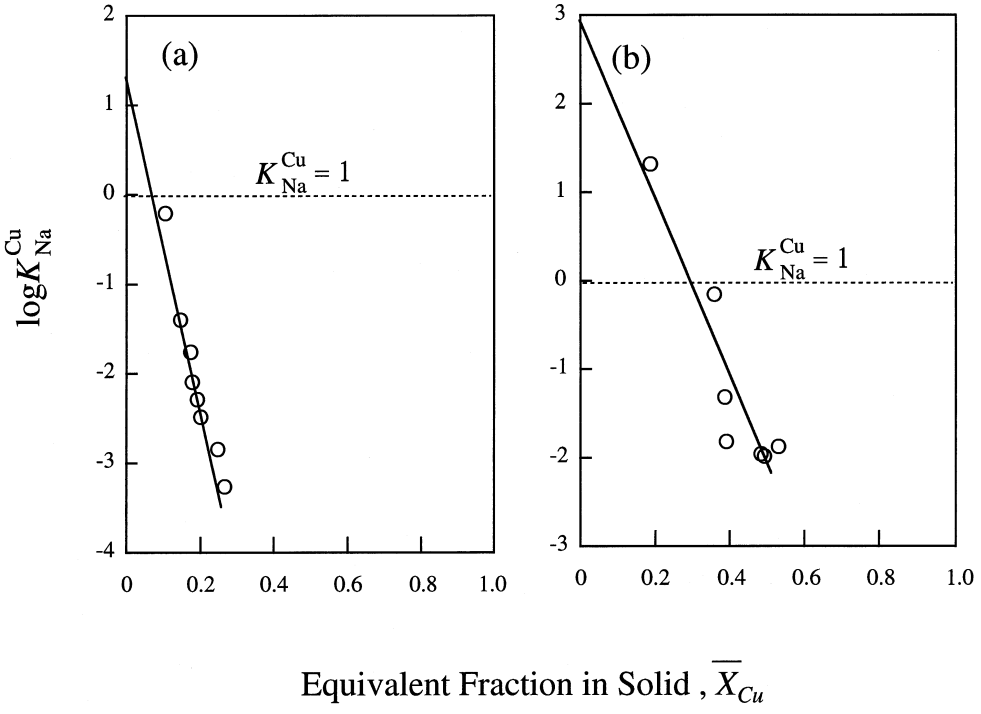

FIG. 4 Kielland plots for $2Na^{+} \rightarrow Cu^{2+}$ exchange on the two different Na–4–micas prepared (a) by solution–sol–gel processing and (b) by crystallization from the mixture of NaF, MgO, and metakaolin precursors.

MARCEL DEKKER, INC.
270 Madison Avenue, New York, New York 10016

TABLE 1
Cation-Exchange Capacities (CECs) and Thermodynamic Data for $2Na^+ \rightarrow M^{2+}$ Exchange on Na-4-mica at Room Temperature

Cation	Sample	CEC for M^{2+}/mequiv $(100\ g)^{-1}$	$\log(K^M_{Na})_{\bar{X}_M \rightarrow 0}$	C_1	$\Delta G°$ ideal/kJ $(equiv)^{-1}$
Cu^{2+}	Solgel-Na-4-mica	122	1.30	−8.98	−2.48
	Metakao-Na-4-mica	225	2.93	−5.05	−7.12
Pb^{2+}	Solgel-Na-4-mica	187	−0.458	1.20	2.55
	Metakao-Na-4-mica	257	0.498	2.18	−0.183

points fall below the dotted line. Na^+ ions are preferred over Cu^{2+} almost throughout the $2Na^+ \rightarrow Cu^{2+}$ exchange.

From the Kielland plots, the $\log(\mathbf{K}^M_{Na})_{\bar{X}_M - 0}$ and the Kielland coefficient C_1 for the initial region of the ion-exchange reaction ($\bar{X}_{Cu} \leq 0.26$ and $\bar{X}_{Cu} \leq 0.53$ for solgel- and metakao-Na-4-micas, respectively) are obtained (Table 1). The $\Delta G°$ for the overall ion-exchange reaction could not be calculated because the Kielland plots were not obtained for high equivalent fractions of copper in the micas ($\bar{X}_{Cu} > 0.26$ and $\bar{X}_{Cu} > 0.53$ for solgel- and metakao-Na-4-micas, respectively). From Eqs. (13) and (14) using $\log(\mathbf{K}^M_{Na})_{\bar{X}_M \rightarrow 0}$, $\Delta G°_{ideal}$ for the $2Na^+ \rightarrow Cu^{2+}$ exchange reactions was estimated and is listed in Table 1. The ion-exchange selectivity for "ideal" exchange with no steric hindrance can be determined from the values of $\Delta G°_{ideal}$. Highly crystallized metakao-Na-4-mica has a much higher selectivity for Cu^{2+} in the ideal exchange in comparison to solgel-Na-4-mica. As mentioned before, the generalized Kielland coefficient, C_1, is related to the energy term for the steric limitation or jumping barrier for exchanging ions in the interlayer and, when the C_1 value is negative, the energy term for the steric limitation is larger because the $|C_1|$ value is larger. The energy term for the steric limitation is also reduced with the highly crystallized metakao-Na-4-mica for the initial region of the ion-exchange reaction.

$2Na^+ \rightarrow Pb^{2+}$ Exchange with the Na-4-micas

Figure 5 shows the isotherms for $2Na^+ \rightarrow Pb^{2+}$ exchange with the two different Na-4-micas. For the solgel-Na-4-mica, the isotherm quickly reaches $\bar{X}_{Pb} = 0.35$ and becomes flat. The isotherm with the metakao-Na-4-mica quickly flattens out when the $\bar{X}_{Pb}$ reaches 0.55. The lead-exchange capacity at $TN = 0.00468$ N was much improved from 187 to 257 mequiv $(100\ g)^{-1}$ with the highly crystallized metakao-Na-4-mica (Table 1), which is from 40 to 59% of the theoretical exchange capacity of Na-4-mica. The Kielland plots for the $2Na^+ \rightarrow Pb^{2+}$ exchange with the two different Na-4-micas are given in Fig. 6.

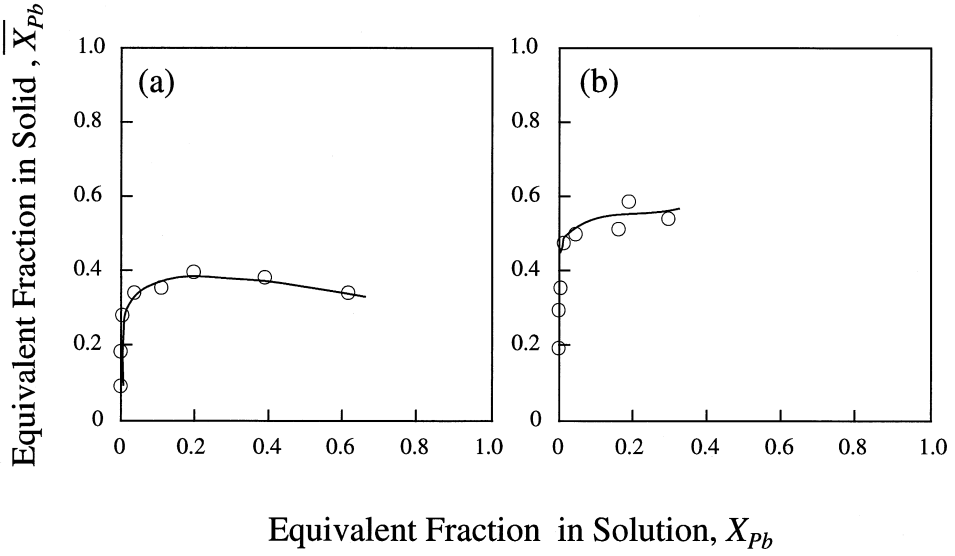

FIG. 5 Cation-exchange isotherms for $2Na^+ \rightarrow Pb^{2+}$ exchange on the two different Na–4–micas prepared (a) by solution–sol–gel processing and (b) by crystallization from the mixture of NaF, MgO, and metakaolin precursors. A total normality of 0.00468 N was used.

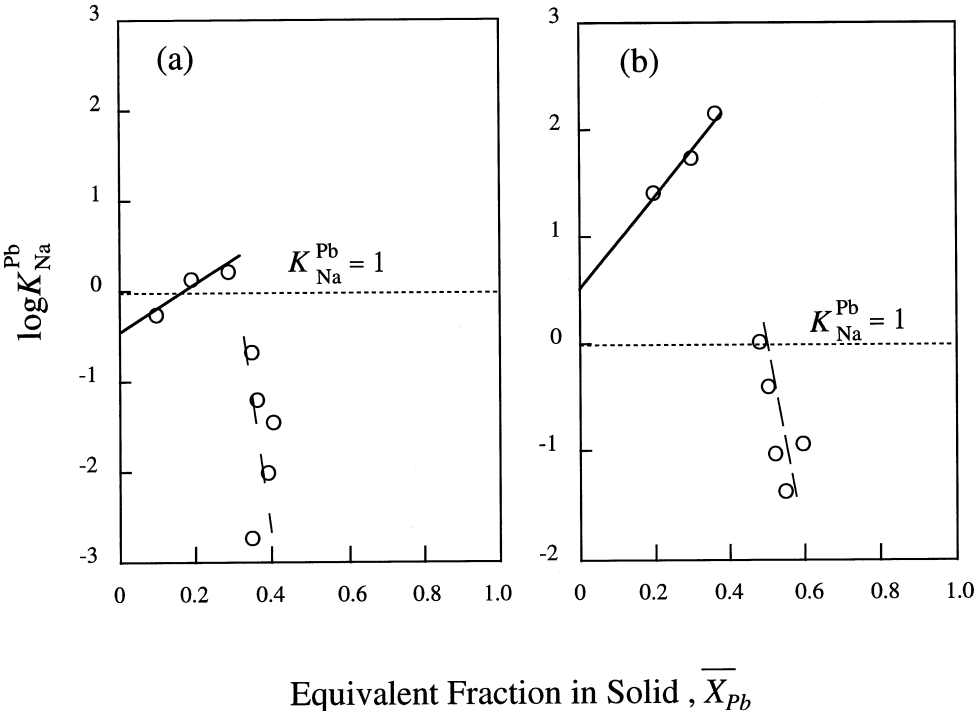

FIG. 6 Kielland plots for $2Na^+ \rightarrow Pb^{2+}$ exchange on the two different Na-4-micas prepared (a) by solution–sol–gel processing and (b) by crystallization from the mixture of NaF, MgO, and metakaolin precursors.

MARCEL DEKKER, INC.
270 Madison Avenue, New York, New York 10016

Break points can be observed in both the isotherms at around $\overline{X}_{Pb} = 0.30$ and 0.40 for the solgel- and metakao-Na-4-micas, respectively. In the initial stage of the lead-exchange reaction, the plots fall above or very close to the dotted line which indicate $K_{Na}^{Pb} = 1$. Pb^{2+} ions are more selective than Na^{+} ions in the initial stage for both Na-4-micas. However, $\overline{X}_{Pb}$ becomes larger than the break point and the corrected selectivity coefficient quickly decreases. The presence of the break point in the $2Na^{+} \rightarrow Pb^{2+}$ exchange isotherm with Na-4-mica is due to the fact that the hydrated interlayer spacing of the Na-4-mica rapidly collapses at $\overline{X}_{Pb} = 0.3$–0.4, as discussed in detail later.

From the Kielland plots, the Kielland coefficient C_1 and $\log(\mathbf{K}_{Na}^{M})_{\overline{X}_M \rightarrow 0}$ for the initial stage of the lead-exchange reaction are obtained (Table 1). The estimated values of ΔG°_{ideal} indicate that highly crystallized metakao-Na-4-mica has a much higher selectivity for Pb^{2+} in the ideal exchange with no steric hindrance for the initial stage of the exchange reaction. It is interesting that the C_1 values are positive in the initial stage, which suggests that the energy term for the steric limitation or jumping barrier is somewhat reduced by the $2Na^{+} \rightarrow Pb^{2+}$ exchange in the initial stage. The values of ΔG° for the lead-exchange reaction could not be obtained here because of the presence of break points in the Kielland plots: ΔG° can be obtained from the integration of the Kielland plot from $\overline{X}_{Pb} = 0$ to $\overline{X}_{Pb} = 1$.

Changes in the Solid Phase of Na-4-mica by the Copper and Lead Exchange

Changes in the solid phase of the ion exchanger were investigated for metakao-Na-4-mica. In the XRD pattern of the copper-exchanged Na-4-mica with $\overline{X}_{Cu} = 0.48$ (Fig. 7a), a strong and broadened peak for (001) reflection appeared along with a large halo at around 24° (CuKα), indicating that the crystallinity gradually decreased as the copper-exchange reaction progressed. On the other hand, in the XRD pattern (Fig. 7b) of the lead-exchanged Na-4-mica with $\overline{X}_{Pb} = 0.59$, the peak of the (001) reflection became very weak and the intensities of the two peaks observed at around $d = 4.1$ and 2.6–2.7 Å became much stronger. Figure 8 shows the changes in the XRD peak for the (001) reflections of the copper- and lead-exchanged Na-4-micas. In the copper-exchange reaction, the (001) reflection peak gradually became broad as the $\overline{X}_{Cu}$ increased, indicating lowering of the crystallinity of the hydrated Na-4-mica (Fig. 7a), but it still remained strong for $\overline{X}_{Cu} \leq 0.53$ (Figs. 8a, b, and c). The basal spacings in the 12.4–13.4 Å range indicate that the interlayer structure of the hydrated Na-4-mica was retained during the copper-exchange reaction. The basal spacings of the copper-exchanged Na-4-micas with $\overline{X}_{Cu} = 0.49$ and 0.53 were $d = 12.5$ and 12.4 which almost corresponds to a structure with a single sheet of interlayer water. For the copper-exchanged Na-4-mica with $\overline{X}_{Cu} = 0.19$, however, the basal spacing increased to 13.4 Å, which may

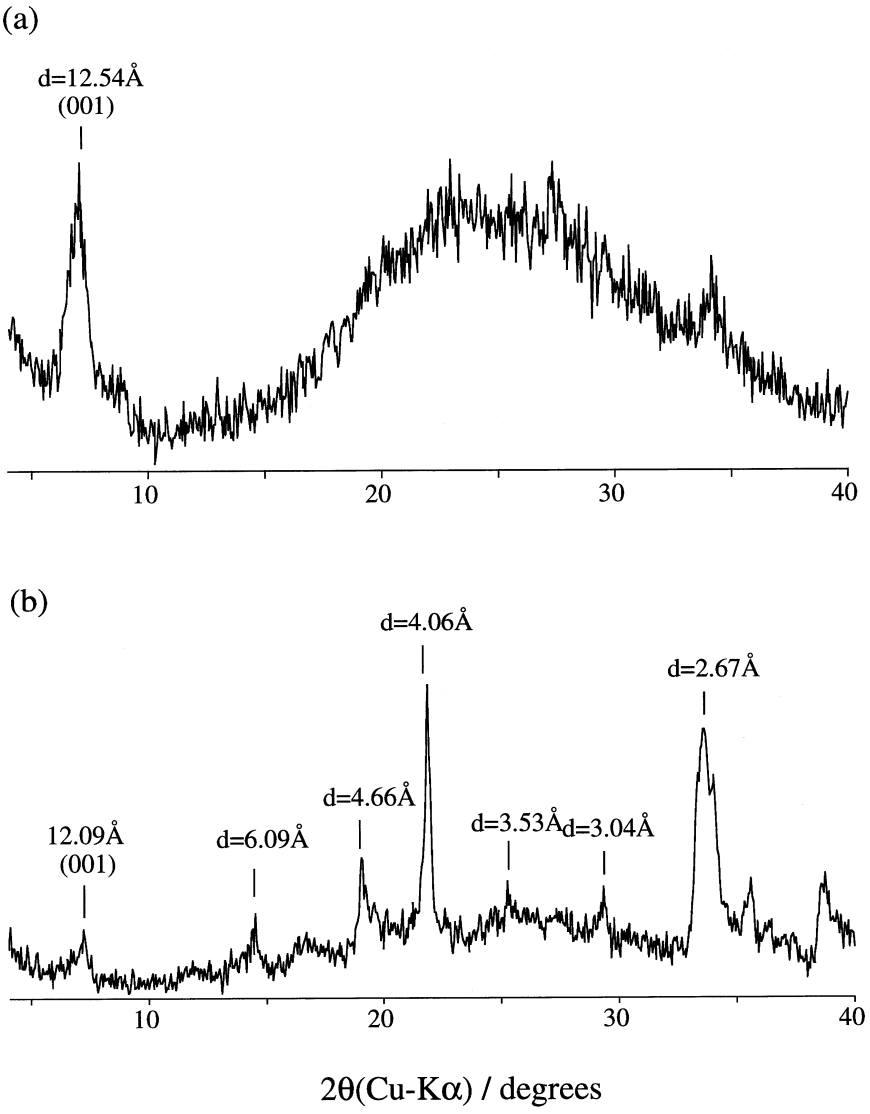

FIG. 7 XRD patterns of (a) the copper-exchanged metakao-Na-4-mica with $\overline{X}_{Cu} = 0.48$ and (b) the lead-exchanged metakao-Na-4-mica with $\overline{X}_{Pb} = 0.59$.

be due to the formation of a structure containing mixed single and double sheets or double sheets of interlayer water. A layer spacing of 13.82 Å was reported on vermiculite prepared by progressive removal of interlayer water from normal vermiculite with double sheets of interlayer water (2). On dehydration of the normal 14.36 Å phase, a 13.82 Å phase was first formed, corresponding to a structure containing double sheets of interlayer water with an arrangement different from that in the 14.36 Å phase. A similar structure of double sheets of interlayer was apparently formed in the Na-4-mica when a small amount of interlayer Na^+ was exchanged by Cu^{2+}. The dehydration of

interlayer water occurred when the $2Na^+ \rightarrow Cu^{2+}$ exchange proceeded to some extent and the double sheets of interlayer water reverted to a single sheet. As shown by Fig. 4, the corrected selectivity coefficient decreased linearly with an increase in the $\overline{X}_{Cu}$ in the copper-exchange reaction, which implies that any significant phase changes, including the collapse of the interlayer spacing of hydrated Na-4-mica, did not occur in the solid, and that the $2Na^+ \rightarrow Cu^{2+}$ exchange proceeded on the interlayer Na^+ sites of hydrated Na-4-mica. [If there is a significant phase change during the copper exchange, the break point will appear in the Kielland plots like the lead exchange (Fig. 6).] The copper exchange gradually became difficult with progressive exchange because steric hindrance gradually increased with $\overline{X}_{Cu}$. The fact that

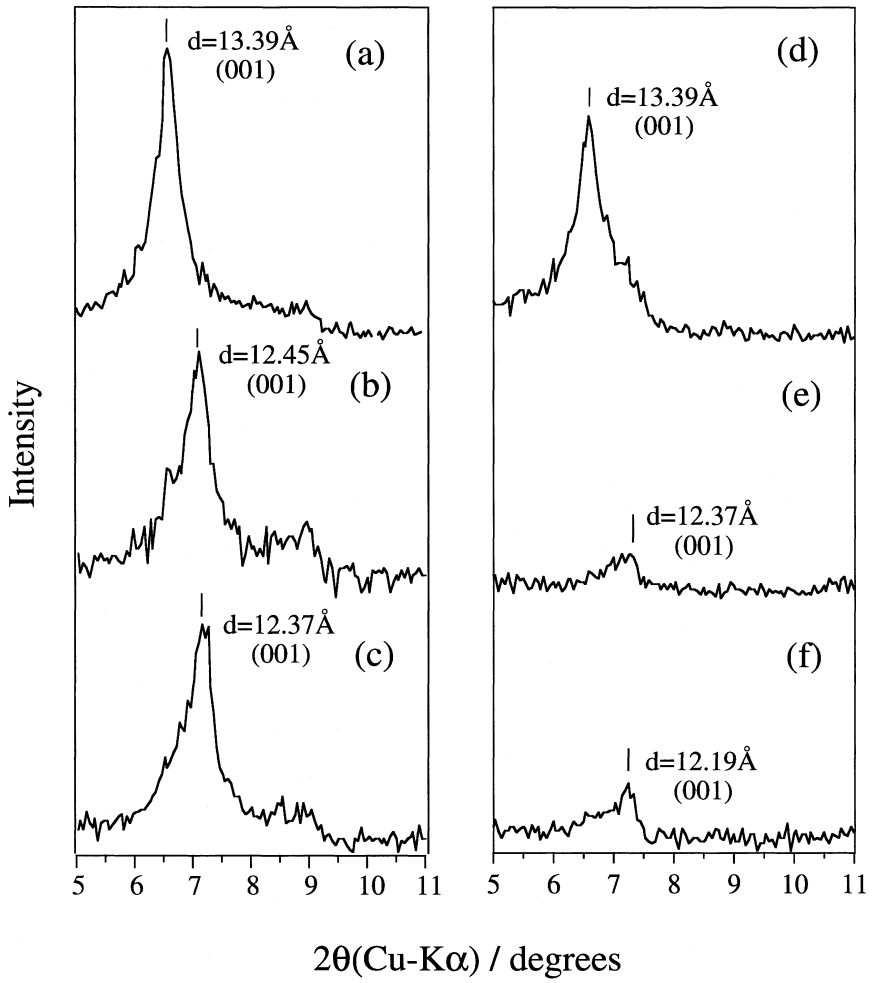

FIG. 8 Changes in XRD peak for (001) reflection of (a)–(c) the copper-exchanged metakao-Na-4-mica and (d)–(f) the lead-exchanged metakao-Na-4-mica. The equivalent fractions of copper and lead in the micas were $\overline{X}_{Cu}$ = (a) 0.19, (b) 0.49, (c) 0.53; $\overline{X}_{Pb}$ = (d) 0.20, (e) 0.52, (f) 0.59.

the layer spacing of the hydrated Na-4-mica gradually lowered (Fig. 8a–c) and the crystallinity of the phase also gradually became poor (Fig. 7a) with increasing $\overline{X}_{Cu}$, makes the steric hindrance larger.

A strong (001) peak was observed in the lead-exchange reaction for $\overline{X}_{Pb} = 0.20$. However, the peak became very weak when $\overline{X}_{Pb} = 0.52$ and 0.59, indicating the collapse of the basal spacing. The equivalent fractions of Cu^{2+} and Pb^{2+} were almost the same between the copper- and lead-exchanged micas given in Figs. 8(c) and 8(e), respectively, but the (001) peak still remains in Fig. 8(c) while it has almost disappeared in Fig. 8(e). The collapse of the hydrated interlayer spacing rapidly occurred when $\overline{X}_{Pb}$ approached a value of about 0.3–0.4. This collapse of the hydrated interlayer spacing leads to the break point in the Kielland plots in Fig. 6; the rapid decrease in the corrected selectivity coefficient at $\overline{X}_{Pb} > 0.3$–0.4 is due to this collapse of the hydrated interlayer structure. Before the collapse took place (the initial stage of the lead exchange), the steric hindrance was rather reduced when the lead exchange progressed as shown by the positive C_1 (Table 1).

One of the present authors previously reported the $2Na^+ \rightarrow Sr^{2+}$ exchange with solgel-Na-4-mica (4). In the strontium exchange the hydrated interlayer spacing also collapsed considerably when about half of the exchange sites were occupied by strontium, as confirmed by powder x-ray diffraction which showed that the *c*-axis decreased from 12.2 to 10.2 Å and that the peak for (001) reflection became very weak and broadened. However, in the $2Na^+ \rightarrow Zn^{2+}$, Ni^{2+}, Cd^{2+}, Co^{2+}, and Mn^{2+} exchanges with metakao-Na-4-mica, the hydrated interlayer structure with basal spacings in the 12.1–13.8 Å range was retained during divalent metal exchange (17). The collapse of the hydrated interlayer spacing by lead or strontium exchange can be explained by the effective ionic radii of the cations as follows. The exchange by cations with a large effective ionic radius, like Pb^{2+} (1.33 Å) and Sr^{2+} (1.32 Å) ions, is believed to cause the collapse of hydrated interlayer spacing when $\overline{X}_M$ becomes large. On the contrary, the hydrated interlayer spacing is almost retained during ion exchange of Zn^{2+} (0.88 Å), Ni^{2+} (0.83 Å), Cd^{2+} (1.09 Å), Co^{2+} (0.89 Å), and Mn^{2+} (0.97 Å) ions, all of which have a smaller effective ionic radius.

CONCLUSIONS

The ion-exchange selectivity of Na-4-mica synthesized cost-effectively from metakaolin was investigated for $2Na^+ \rightarrow Cu^{2+}$ or Pb^{2+} exchange in comparison to that of solution–sol–gel processed Na-4-mica. Na-4-mica with a higher crystallinity could be prepared by the crystallization from a mixture of NaF, MgO, and metakaolin in comparison to that prepared by solution–sol–gel processing. This high crystallinity of Na-4-mica may be due to the fact that it is favorably crystallized in the matrix of a skeleton structure

MARCEL DEKKER, INC.
270 Madison Avenue, New York, New York 10016

of metakaolin as a precursor of Al and Si mixed at the atomic level. Selectivities for copper and lead exchange with Na-4-mica in the initial ion-exchange reaction were improved with the highly crystallized Na-4-mica from metakaolin. Large cation-exchange capacities of 225 and 257 mequiv $(100\ g)^{-1}$ could be obtained for Cu^{2+} and Pb^{2+}, respectively. Swelling sodium micas of the true mica type were recently prepared from naturally occurring phlogopite mica at room temperature by using sodium tetraphenyl boron (18) and from phlogopite and biotite by repeated hydrothermal treatments with 2 M NaCl at 180°C for 18 hours (19). The former authors (18) showed there were very high selectivities for cesium while the latter authors (19) showed there were high selectivities for Pb and Cu with uptakes of almost 150 mequiv $(100\ g)^{-1}$ (about 2/3 of the theoretical capacity). Our brittle mica showed 1.5–1.7 times Pb and Cu uptakes in comparison to these micas from natural phlogopite and biotite. Fluorinated clays have been commercially prepared since the early 1950s by solid-state methods because of the simplicity of the process; solution methods (18, 19) have not yet been commercialized. The particle size, morphology, homogeneity, and crystallinity, all of which improve the ion-exchange properties, may be controlled for our synthetic mica by changing the synthetic conditions.

The basal spacing of the hydrated phase of Na-4-mica rapidly collapsed when the equivalent fraction of Pb^{2+} in the mica became large ($\overline{X}_{Pb} > 0.40$ for metakao-Na-4-mica). On the other hand, it was retained in the copper-exchange reaction ($\overline{X}_{Cu} \leq 0.53$ for metakao-Na-4-mica) although the crystallinity of the hydrated Na-4-mica became less and the hydrated interlayer spacing was somewhat lowered. This difference in the stability of the hydrated interlayer structure may be explained by the effective ionic radii of the cations. The thermodynamic functions for the initial ion-exchange equilibria at room temperature were also calculated.

ACKNOWLEDGMENT

This work was supported by the Interfacial, Transport and Separation Program, Chemical and Transport Systems, Division of the National Science Foundation under Grant CTS-9612714.

REFERENCES

1. R. M. Barrer, *Zeolites and Clay Minerals as Sorbents and Molecular Sieves*, Academic Press, London, 1978, p. 497.
2. R. E. Grim, *Clay Mineralogy*, 2nd ed., McGraw-Hill, New York, NY 1968, pp. 33, 188, and 104.
3. M. Gregorkiewitz, J. F. Alcover, J. A. Rausell-Colom, and J. M. Serratosa, *2eme Reunion des Groupes Europeens d'Argiles*, Strasbourg, 1974, p. 64.
4. W. J. Paulus, S. Komarneni, and R. Roy, *Nature (London), 357*, 571 (1992).

5. S. Komarneni, W. J. Paulus, and R. Roy, in *New Developments in Ion Exchange; Proceedings of an International Conference on Ion Exchange*, Elsevier, Amsterdam, 1991, p. 51.
6. K. R. Franklin and E. Lee, *J. Mater. Chem.*, *6*, 109 (1996).
7. S. Komarneni, R. Pidugu, and J. E. Amonette, *Ibid.*, *8*, 205 (1998).
8. R. M. Barrer and J. Klinowski, *J. Chem. Soc., Faraday Trans. I*, *70*, 2080 (1974).
9. F. Helfferich, *Ion Exchange*, Dover, New York, NY, 1995, p. 170.
10. J. Kielland, *J. Soc. Chem. Ind.*, *54*, 232T (1935).
11. E. Ekedahl, E. Högfeldt, and L. G. Sillén, *Acta Chem. Scand.*, *4*, 556 (1950).
12. G. L. Gaines Jr. and H. C. Thomas, *J. Chem. Phys.*, *21*, 714 (1953).
13. R. M. Barrer and J. D. Falconer, *Proc. R. Soc. London A*, *236*, 227 (1956).
14. R. M. Barrer, *Natural Zeolites, Occurrence, Properties and Use*, Pergamon, Oxford, 1978, p. 385.
15. M. Tsuji, H. Kaneko, and Y. Tamaura, *J. Chem. Soc., Faraday Trans.*, *89*, 851 (1993).
16. Y. Tanaka and M. Tsuji, *Mater. Res. Bull.*, *32*, 461 (1997).
17. T. Kodama and S. Komarneni, *J. Mater. Chem.*, *9*, 533 (1999).
18. S. Komarneni and R. Roy, *Science*, *239*, 1286 (1988).
19. A. I. Bortun, L. N. Bortun, S. A. Khainakov, and A. Clearfield, *Solv. Extr. Ion Exch.*, *16*, 1067 (1998).

Received by editor September 20, 1998
Revision received January 1999

Request Permission or Order Reprints Instantly!